Al-Khwarizmi Engineering Journal, Vol. 18, No. 3, September, (2022)
P. P. 1- 14

Al-Khwarizmi Engineering Journal

Design and Analysis of a Spraying Robot

Fatima M. Jasim* **Malik M. Ali****
Ali H. Hamad***

*,**Department of Mechatronics Engineering/ Al-khwarizmi College of Engineering/ University of Baghdad/ Baghdad/ Iraq
***Department of Information and Communication Engineering/ Al-khwarizmi College of Engineering/ University of Baghdad/ Baghdad/ Iraq
*Email: fatomaa.eng@gmail.com
**Email: malik@kecbu.uobaghdad.edu.iq
***Email: ahamad@kecbu.uobaghdad.edu.iq

(Received 28 March 2022; Accepted 3 July 2022)
https://doi.org/10.22153/kej.2022.07.001

Abstract

An indoor spraying robot is built in this research to solve numerous challenges associated with manual spraying. The mechanical, hardware and essential technologies used are all detailed and designed. The proposed spraying robot's conceptual design is split into two parts: hardware and software. The mechanical design, manufacturing, electrical, and electronics systems are described in the hardware part, while the control of the robot is described in the software section. This robot's kinematic and dynamic models were developed using three links that move in the x, y, and z directions. The robot was then designed using SolidWorks software to compute each connection's deflection and maximum stresses. The characteristics of the stepper motors, power screw and belt drive, are calculated. Finally, an Arduino-Nano controller and stepper motor actuators were used to build and run the robot. As a result, the robot was able to move smoothly vertically and horizontally, according to the findings of the experiments as shown in figures 22, 23, 24, and 25. These figures showed the position and velocity curves of the links of the robot.

Keywords: *Cartesian Robot, Kinematic, Dynamic, system design.*

1. Introduction

During the development of science and technology, industrial robots appeared in industrial operations. Industrial robots are electromechanical devices that can perform industrial tasks accurately; besides that, they are used to reduce the risks of industrial processes for humans in continuous work and reduce the consumption of materials. Industrial robots can move in rotary motions such as articulated, SCARA, cylindrical, spherical or linear motion. The Cartesian robot is also called a rectilinear or gantry robot. It has three linear joints (or a combination of them) that use the Cartesian coordinate system (X, Y, and Z). This robot may also have an attached wrist to allow for rotational movement. The prismatic joints deliver linear motions along the respective axes. This robot is employed in material handling, computer numeric control machine load/unload, spraying materials, etc. The spraying operation is one of the essential processes in industrial robots, the most important of which is spraying for painting walls, cars, and devices and spraying insecticides on plants to get rid of agricultural pests and others. Also, they are used in purgation hospitals to prevent viruses. Therefore, the use of industrial robots to spray instead of humans is vital to caring for the health of the human body because it is affected by the paint and ventilation conditions of the spraying room. Furthermore, these robots also achieve a good quality of the spray-painting of the products. In (2013), [1] review the works related to

coating thickness problems and improving the multi-objective constraint. However, it did develop methods for modeling the deposition of materials such as Gaussian, Cauchy, Parabolic, and Beta models, but it did not come with satisfactory results. Fortunately, the min-max method has proven itself in formulating the paint film function for free-form surfaces. The appropriate tool path within an appropriate time and membrane quantity deviation was also inferred. From this data, the paint deposition rate model algorithm and the assumption of the gun shape of the paint like a cone were available. In 2015, [2] compare the cost and risks of hand painting over painting robots, a three-axis (X, Y, and Z) with a two-part Cartesian robot controlled by a PLC and a computer was implemented. The first part is the unit of movement of the three axes x, y and z. Each axis contains a single-phase motor and transmission mechanisms and sensors to control motion. The second is the coating unit created by a pneumatic system. In 2015 [3], The robot chassis was developed to suit painting and interior wall decoration works, and it consists of 8dof, of which 6dof are robotic arms mounted on a 2dof movable base which are connected to it by four points of wheels. The differential system was driven, and a kinematic model of the robot joints was shown, and through the resulting matrix from the Jacobin matrix, the movement was planned and controlled. In 2017 [4] suggested a mathematical spray model of robot painting system based on Gaussian distribution intensity of spray painting operation, it also compared a characters of color-intensity when changing the distance between airbrush and painting surface within the spraying time. In 2017, a gantry robot derived a mathematical and dynamic model using a bond graph technique. Furthermore, the robot has simulated its motion on MATLAB within SolidWorks design and it was using a quadratic function with a velocity profile called a trajectory plan of the robot as in [5]. In 2019 [6], the dynamic model obtained the appropriate inertia parameters of the Kuka LWR robot and its final efficacy. The geometric parameters also distinguished as shown in the tables the fastest time by defining those parameters as the joint torque was estimated with the RMS difference. Based on the robot's self-sensing, the force sensor was replaced by an estimate of the external forces applied, and the torque was related to the Jacobin matrix. The kinetic accuracy clarified the accuracy of the external forces. In (2020) [7], a suitable material was proposed to design industrial robots, especially spray-painting robots. So, it had agreed to choose aluminum alloy to create the arm to reduce the weight of the portable arm and to choose steel alloy in the design of the base because it requires high rigidity and strength. In (2021) [8], a painting mobile robot was designed to avoid accidents of painting buildings on humans. The structure is designed from a moving part with a spray gun using two Arduino UNO boards connected wirelessly (to get rid of the burden of long electrical wires). First, the robot detects the area to be painted and completes it with high accuracy on its own. Next, the robot moves through the DC motor to move the four wheels, where the position of the wall to be painted is detected using the ultrasonic sensor. Then the spray gun paints the wall either horizontally or vertically. This paper presents the kinematic and dynamic model of the 3-DOF Cartesian robot (X, Y, and Z) for painting wall operation and analyzes robot fabrication for each link of it. In addition, the mechanical structure of this robot with its details is discussed. Section 2 presents the derivation of the kinematic and dynamic model of the 3-DOF Cartesian robot. Section 3 explains the mechanical structure and electronic circuit design. Finally, section 4 discusses the numerical and graphic results of the proposed models and the experimental results of the movement.

2. Mathematical Models

2.1 Kinematic Model

The robot manipulator is designed by a set of links that are connected within by joints which are revolute or prismatic, so n joints will haven + 1 links, because each joint connects two links. With the joint, there is a joint variable, denoted by q_i. In the case of a revolute joint, qi is the angle of rotation, and in the case of a prismatic joint, qi is the joint displacement [9].

The kinematic model represents the motion of each link without respect to force; However, the forward kinematics model is an analysis that gives the relationship between the individual joints of the robot and the position and orientation of the end-effector. Denavit-Hartenberg's (DH) method finds a forward kinematic consisting of four variables for each link, such as a, d, Θ, and α [14] and [15]. a is the link length, d is the link offset, Θ is the joint angle, and α is the joint twist [10]. A manipulator whose first three joints are prismatic is a Cartesian manipulator. It has Cartesian coordinates representing the joint variables—the structure and workspace of the robot are shown in figures 1 and 2.

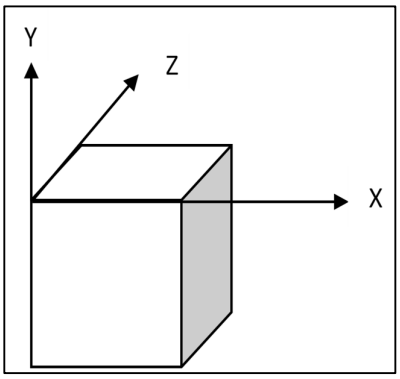

Fig. 1. Workspace of Cartesian robot.

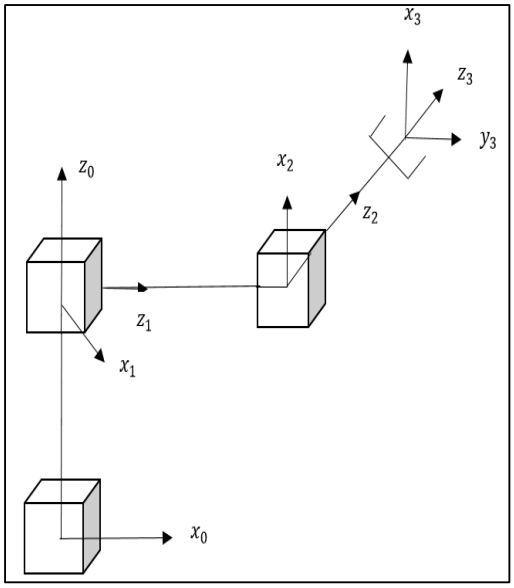

Fig. 2. Three links Cartesian robot.

Table 1,
D-H parameters of robot.

a	D	α	θ
0	q_1	-90	-90
0	q_2	90	-90
0	q_3	0	0

From above table matrices of each link is obtained as follow:

$$T_1^0=\begin{bmatrix}1&0&0&0\\0&1&0&0\\0&0&1&q_1\\0&0&0&1\end{bmatrix},$$

$$T_2^1=\begin{bmatrix}1&0&0&0\\0&1&0&0\\0&0&1&q_2\\0&0&0&1\end{bmatrix},$$

$$T_3^2=\begin{bmatrix}1&0&0&0\\0&1&0&0\\0&0&1&q_3\\0&0&0&1\end{bmatrix}$$

Where T is the transformation matrix for the axes of frame $O_1\ x_1y_1z_1$ (last frame) with respect to the coordinate frame $O_0\ x_0y_0z_0$ (previous frame).

The transformation matrix of the end-effector to the reference frame is concluded by multiplying the previous matrices, so

$$T_i^0= T_1^0 \times T_2^1 \times T_3^2 \quad \ldots(1)$$

$$T_3^0=\begin{bmatrix}1&0&0&q_3\\0&1&0&q_2\\0&0&1&q_1\\0&0&0&1\end{bmatrix}$$

Where $q_1, q_2, and\ q_3$ are the joint space of each link. Joint velocity and acceleration of end-effector are determined with respect to the base frame, hence:

$$V_3^0= \dot{q}_{3i}- \dot{q}_{2j} + \dot{q}_{1k} \quad \ldots(2)$$

$$a_3^0 = (\ddot{q}_3-g)\ i - \ddot{q}_{2j}+ \ddot{q}_{1k} \quad \ldots(3)$$

Where g is the gravitational acceleration, $\dot{q}$ is the joint velocity of links, and $\ddot{q}$ is the joint acceleration.

2.2 Dynamic model

From the dynamic model, the equation of motion is achieved. Besides that, the system's response can be obtained by using the state-space model found from the dynamic model [11] and [16]. There are several techniques to find dynamic equations in robot manipulators, such as the Newton-Euler equations.

$$m_1\ddot{q}_{y_1} = F_1- b_1\dot{q}_{y_1} \quad \ldots(4)$$

$$m_2\ddot{q}_{x_1} = F_2- b_2\dot{q}_{x_1} - k_2q_{x_1} \quad \ldots(5)$$

$$m_3\ddot{q}_{z_1} = F_3- b_3\dot{q}_{z_1} \quad \ldots(6)$$

Where m_1, q_{y_1}, $\dot{q}_{y_1}$, $\ddot{q}_{y_1}$, b_1, and F_1 are the mass, joint position, joint velocity, joint acceleration, damper coefficient, and force applied respectively, and k_2 is the stiffness coefficient of second link that is caused by the belt.

The subscript y1, x1, and z1 represent the first link, second link and the third link.

To derive the dynamic model of robot manipulator, the masses are weight using a suitable scale. This robot has three masses moving vertically and two masses moving horizontally, subsequently [9].

$$\begin{bmatrix}(m_1+m_2+m_3)&0&0\\0&(m_2+m_3)&0\\0&0&m_3\end{bmatrix}\begin{Bmatrix}\ddot{q}_{y_1}+g\\\ddot{q}_{x_1}\\\ddot{q}_{z_1}\end{Bmatrix}+\begin{bmatrix}b_1&0&0\\0&b_2&0\\0&0&b_3\end{bmatrix}\begin{Bmatrix}\dot{q}_{y_1}\\\dot{q}_{x_1}\\\dot{q}_{z_1}\end{Bmatrix}+\begin{bmatrix}0&0&0\\0&K_2&0\\0&0&0\end{bmatrix}\begin{Bmatrix}q_{y_1}\\q_{x_1}\\q_{z_1}\end{Bmatrix}=\begin{bmatrix}F_1\\F_2\\F_3\end{bmatrix} \quad \ldots(7)$$

Above are the equations of motion of each link; however, those equations can be simulated by using the state-space model as follows:

$$q_{y_2} = \dot{q}_{y_1} \quad ...(8)$$

$$q_{x_2} = \dot{q}_{x_1} \quad ...(9)$$

$$q_{z_2} = \dot{q}_{z_1} \quad ...(10)$$

The state space formula given by:

$$\dot{X} = A\,X + B\,u \quad ...(11)$$

The output of the proposed system is the position of the end-effector for Cartesian coordinates (X, Y, and Z of robot links) are obtained through the equation below:

$$Y = C\,X + D\,u \quad ...(12)$$

From equation 11 the state space model for Cartesian robot is given by:

$$\begin{bmatrix} \dot{q}_{y_1} \\ \dot{q}_{y_2} \\ \dot{q}_{x_1} \\ \dot{q}_{x_2} \\ \dot{q}_{z_1} \\ \dot{q}_{z_2} \end{bmatrix} = \begin{bmatrix} 0 & 1 & 0 & 0 & 0 & 0 \\ 0 & \left(\frac{-b_1}{m_1+m_2+m_3}\right) & 0 & 0 & 0 & 0 \\ 0 & 0 & 0 & 1 & 0 & 0 \\ 0 & 0 & \left(\frac{-K_2}{m_2+m_3}\right) & \left(\frac{-b_2}{m_2+m_3}\right) & 0 & 0 \\ 0 & 0 & 0 & 0 & 0 & 1 \\ 0 & 0 & 0 & 0 & 0 & \left(\frac{-b3}{m_3}\right) \end{bmatrix} \begin{Bmatrix} q_{y_1} \\ q_{y_2} \\ q_{x_1} \\ q_{x_2} \\ q_{z_1} \\ q_{z_2} \end{Bmatrix} + \begin{bmatrix} 0 & 0 & 0 & 0 & 0 & 0 \\ 0 & \left(\frac{1}{m_1+m_2+m_3}\right) & 0 & 0 & 0 & 0 \\ 0 & 0 & 0 & 0 & 0 & 0 \\ 0 & 0 & 0 & \left(\frac{1}{m_2+m_3}\right) & 0 & 0 \\ 0 & 0 & 0 & 0 & 0 & 0 \\ 0 & 0 & 0 & 0 & 0 & \left(\frac{1}{m_3}\right) \end{bmatrix} \begin{Bmatrix} 0 \\ F_1 - (m_1+m_2+m_3)g \\ 0 \\ F_2 \\ 0 \\ F_3 \end{Bmatrix} \quad ...(13)$$

3. Design of The Cartesian Robot

3.1 The Structure of Cartesian Robot

The Cartesian robot is designed with three links in the X-direction, Y-direction, and Z-direction. This robot is designed for wall operations, as shown in fig.3; the structure of the Cartesian robot was designed with the help of SolidWorks software. The first link moves in the Y-direction, ranging from 0 to 90 cm. Two stepper motors create the motion; each one has a maximum power equal to 18 Watts and transforms rotational motion to linear motion by using two lead screws, as shown in fig.4. The link choice for the structure is made from an aluminum beam that is 2040 V-Slot type made from 6063-T5 Aluminum material, because it achieves a rigid and lightweight frame, as shown in Fig.5. The mechanical specifications are listed in Table 2.

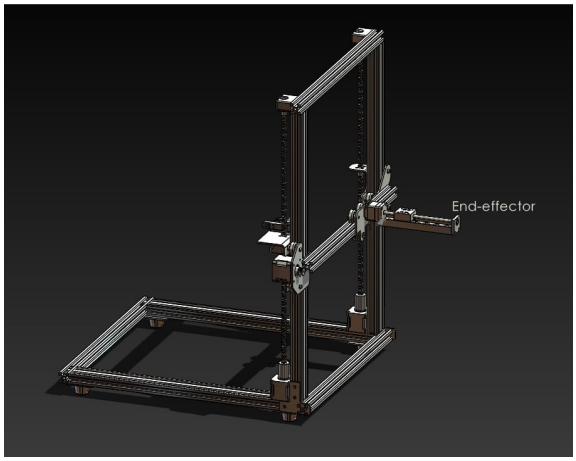

Fig. 3. Structural design of robot in SolidWorks.

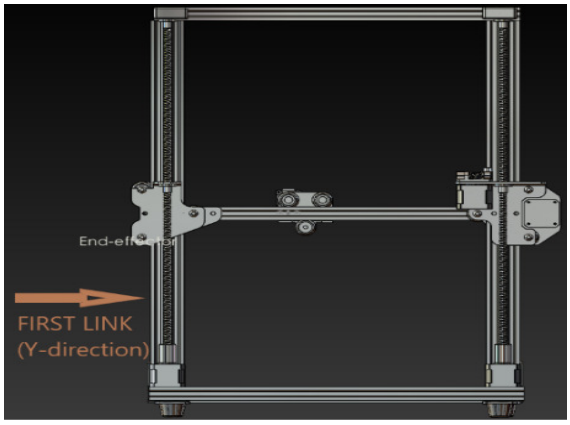

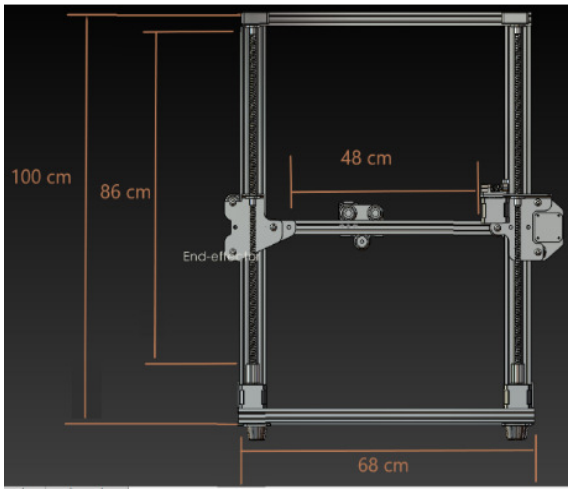

Fig. 4. Front view of the first link.

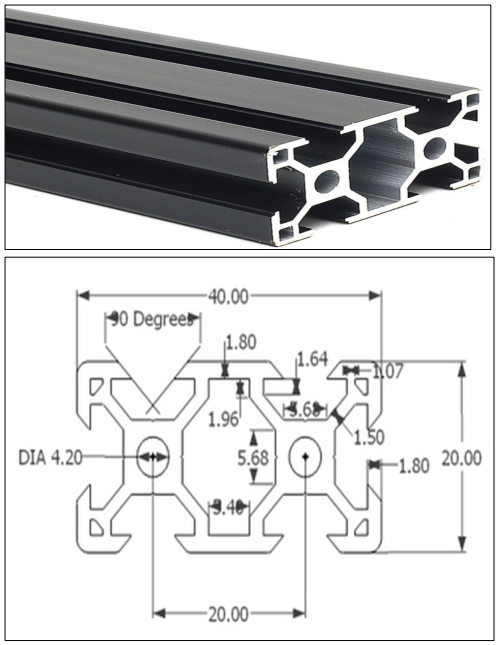

Fig. 5. Aluminum profile 2040 for first link.

Table 2,
Mechanical properties of Aluminum profile 2040

Property	Value
Profile dimensions	20x40 mm
Slot width	6mm
Slot depth	6mm
Weight	0.5 kg/m
Available sizes	do 3000 mm
Thickness	0.30mm-Customized
Mass of inertia(Ix)	$4.64cm^4$
Mass of inertia(Iy)	$1.42cm^4$
Section modulus(Zx)	$2.32cm^3$
Section modulus(Zy)	$1.32cm^3$
Working tension	2.205N/mm
Product force	110MPa

The vertical beams may be exposed to buckling, so the critical load of each beam is calculated as equal to 8005.99N. Next, the maximum stress and deflection of each beam is calculated by using SolidWorks software, as shown in figs 6 and 7. The lead screw that transforms rotational motion to linear motion is made from stainless steel and connected with a brass copper nut. The capacity and basic life of lead screw are obtained by SolidWorks, as shown in figs 8 and 9. Also, the standard parameters of the chosen lead screw are indicated in Table 3.

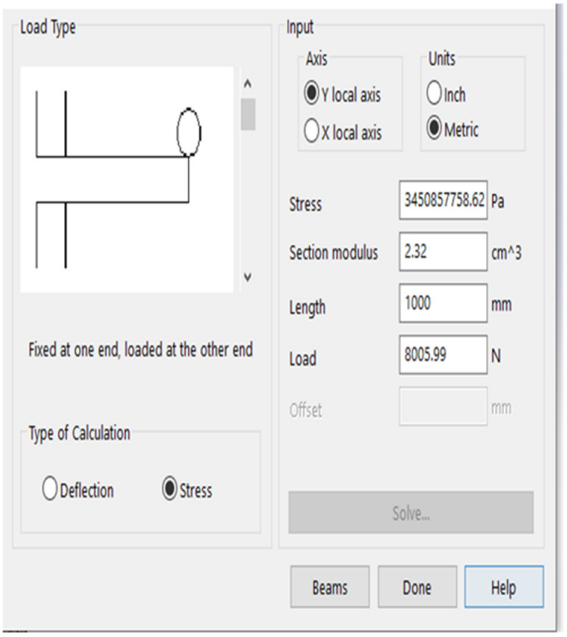

Fig. 6. Stress calculation of first link beams.

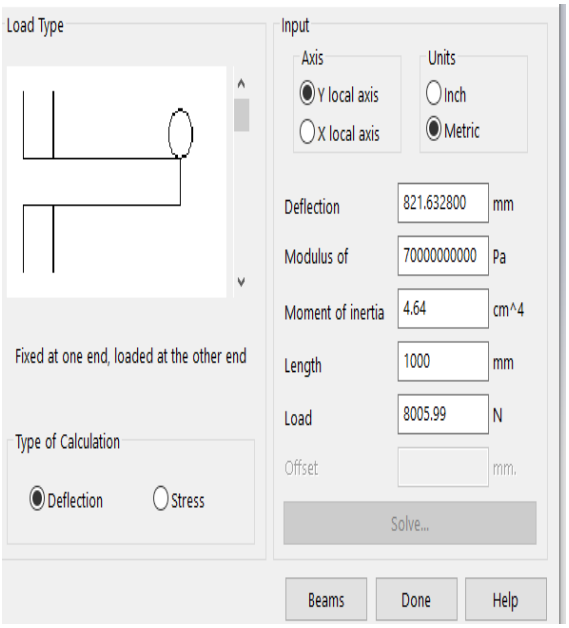

Fig. 7. Deflection calculation of first link beams.

Fig. 8. Stainless steel lead screw.

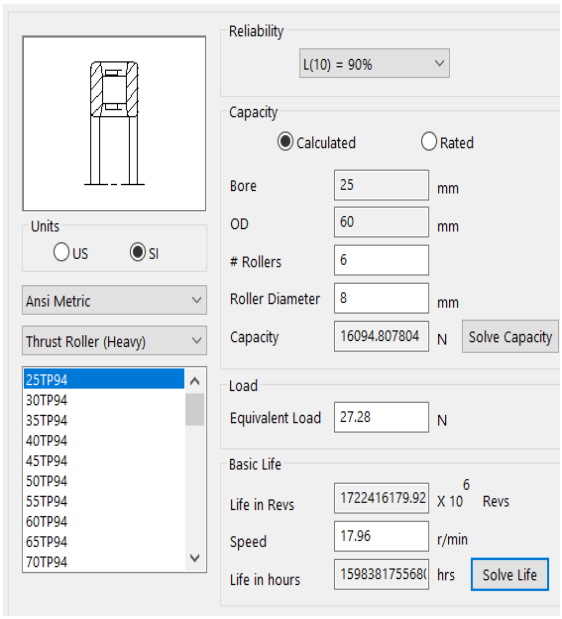

Fig. 9. SolidWorks calculation of Stainless screw.

Table 3,
Parameters of lead screw.

Parameters	Value
Pitch	2mm
Outer Diameter	8mm
Coefficient of friction for screw (μ_1)	0,08
Coefficient of friction for nut (μ_2)	0.06
Nut diameter	20mm

The second link of the robot moves a 48cm range horizontally in the X-direction. This motion is created by on stepper motor with a maximum power of 20.4 watts. The link was made from the same aluminum beam as the first link, and the belt drive is transformed from rotational motion to linear motion, as shown in Fig.10. The horizontal beam that carries the X and Z link in this system bears the overall load, so, the maximum stress and deflection are 1.6876 mm, and 12.6013 MPa, as shown in figs 11 and 12. The belt used in the X-direction to achieve the smoothest-movement is called 2GT timing belt (flat belt), as shown in Fig.13 and Table 4.

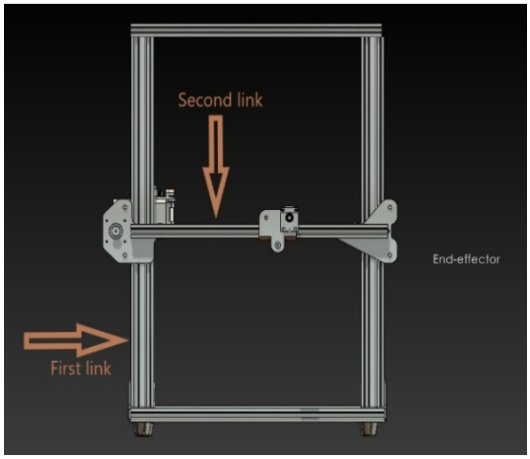

Fig. 10. Front view of the second link of the robot.

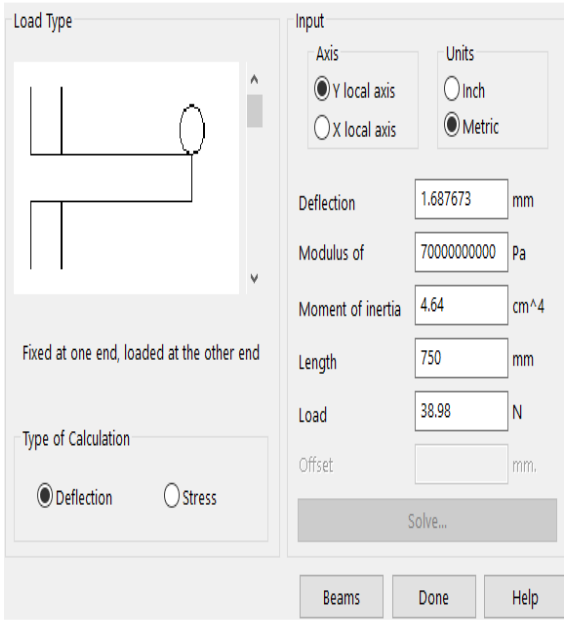

Fig. 11. Deflection calculation of second link beam.

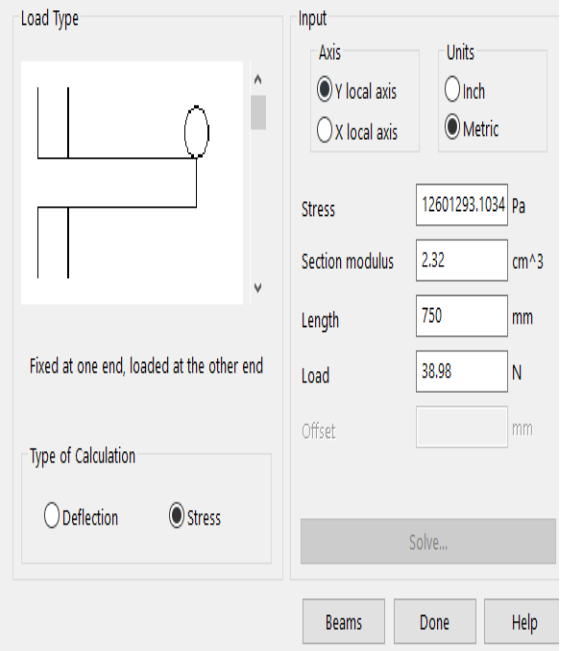

Fig. 12. Stress calculation of second link beam.

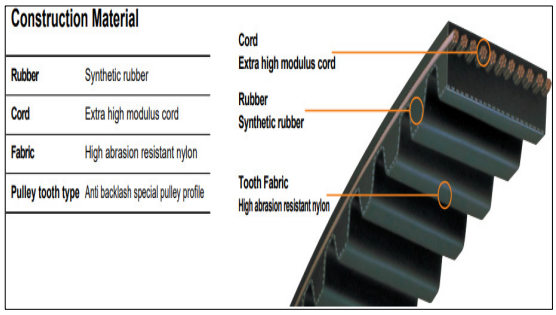

Fig. 13. GT2 Timing belt structure.

Table 4,
The specifications of belt.

Specification	Value
Pitch	2mm
Width	6mm
Length	160cm
Height	1.38mm
Tooth height	0.75mm
Breaking strength	0.55158KN
Working tension	0.027801KN
Modulus of elasticity	0.05 GPa

The final link of the robot moves in the Z-direction with a 30cm range. This link is manufactured the same as the first link, i.e. the same beam and screw, as shown in Fig.14. The assembly structure of the robot is shown in Fig.15.

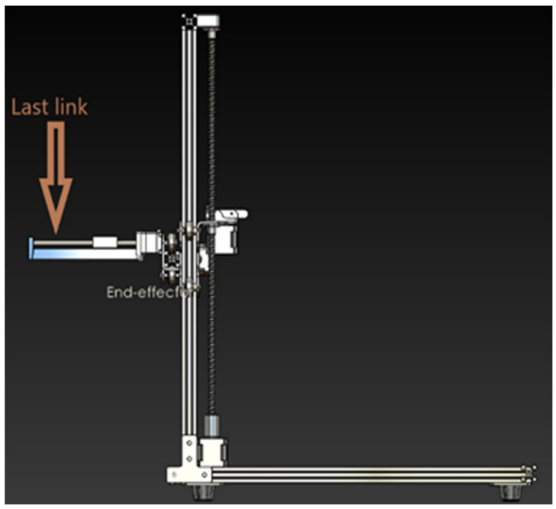

Fig. 14. Side view for the final link of the robot.

Fig. 15 The structure of Cartesian robot.

3.2 Electrical and electronic design

The robot should move in a smooth and accurate movement. To achieve that, a particular motor like a stepper motor was used to indicate precise and calculated steps without building a complex control system. This motor has a high-power density and is capable of high micro-step resolution and quiet operation with minimal resonance. The Bipolar type of this motor is used to obtain direction and effort. To control a stepper

motor, an Arduino-Nano connects to the driver (DRV8825) for the stepper motor, as shown in Fig.16. The stepper motor specifications are shown in Table 5, and the block diagram of the electrical circuit of the robot is shown in Fig17.

Table 5,
Hybrid Stepper motor features

Feature	17HS1538 (X&Z-link)	17HS1600 (Y-link)
Maximum axial force	10N	10N
Maximum radial force	28N	28N
Holding torque	0.45 N.m	0.80 N.m
Step angle	1.8º	1.8º
Operating voltage	12volt	12volt
Rated current	1.7 ampere	1.5 ampere
Weight	320g	550g
Inductance	3.2 m.H/Phase	7.0 m.H/Phase
Insulation resistance	100 mΩ,/500VDC	100 mΩ,/500VDC
Dielectric strength	500 VAC	500 VAC
Rotor inertia	54 g.cm^2	102 g.cm^2
Shaft radial play	0.2 max	0.2 max
Shaft Diameter	5mm	5mm
Shaft axial play	0.8 max	0.8 max

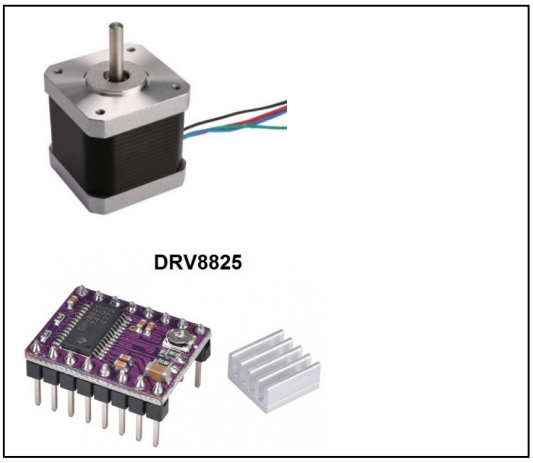

Fig. 16 Stepper motor nema17 and its driver.

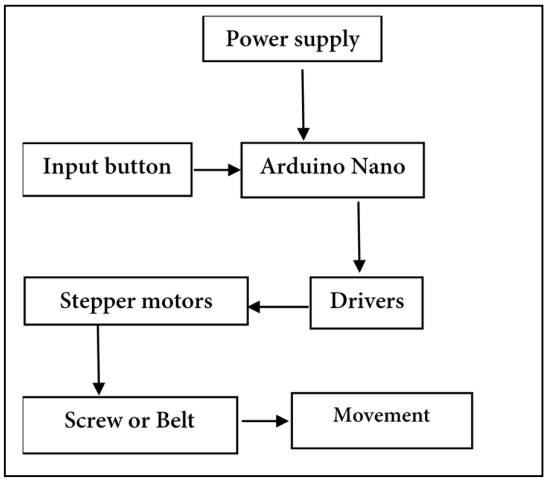

Fig. 17. Block diagram of motion sequence.

4. Experimental and Simulation Results

4.1 Stepper motor results

The characteristics of the stepper motor are calculated and shown in table 6. It can be observed that the motor's powers are different depending on the position and the load that carries it out.

Table 6,
17HS6001 and 17HS1538 motors calculations.

Term	17HS6001 (X&Z-link)	17HS1538 (Y-link)
Maximum speed(N_i)	2.86 rev/sec	5.51 rev/sec
Step per revolution	200 step/rev	200 step/rev
Minimum time step	1.75 ms	0.907 ms
Maximum power	18 watt	20.4 watt
Angular velocity	17.96 rad/sec	34.6 rad/sec

4.2 Lead screw and belt results

The terms of power screw and belt drive are determined by standard equations in [12] and these values are shown in tables 7 and 8.

Table 7,
Lead screw of first link and last link results.

Term	Y-link screw	Z-link screw
Load (W_1)	27.28 N	7.85 N
Force applied(F_{s1})	4.365 N	1.26 N
$Torque_1$	28.92 N.mm	8.34 N.mm
Power (P_1)	519.4 watt	288.56 watt
helix angle	4.516985	4.516985
Average diameter(R)	7mm	7mm

Table 8,
Belt of second link results.

Term	Value	
Load (W_1)	15mm	
Force applied(F_{s1})	4.365 N	1.26 N
$Torque_1$	28.92 N.mm	8.34 N.mm
Power (P_1)	519.4 watt	288.56 watt
helix angle	4.516985	4.516985
Average diameter(R)	7mm	7mm

4.3 Simulation results

4.3.1 Kinematic model response

When entering the DH parameters of the robot in MATLAB, we can conclude the plot directions of the robot's links and the robot's path, as shown in fig. 18 and fig.19. Figure 18 shows the robot's configuration in three dimensions and the end-effector's initial position, while Figure 19 shows the path of the robot motion for two cycles.

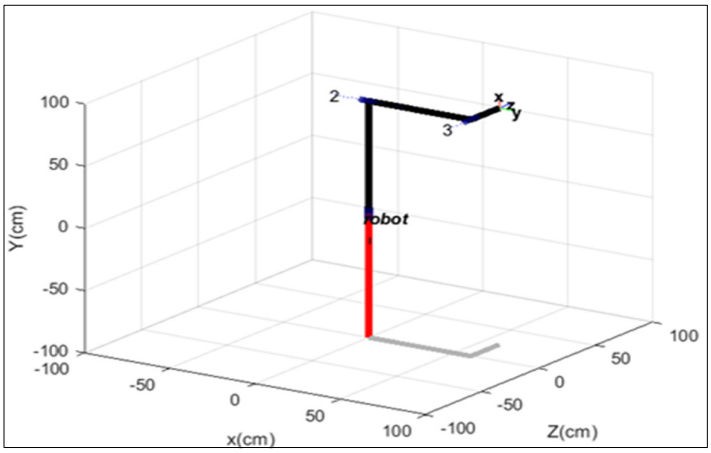

Fig. 18. Simulation of Cartesian robot on MATLAB.

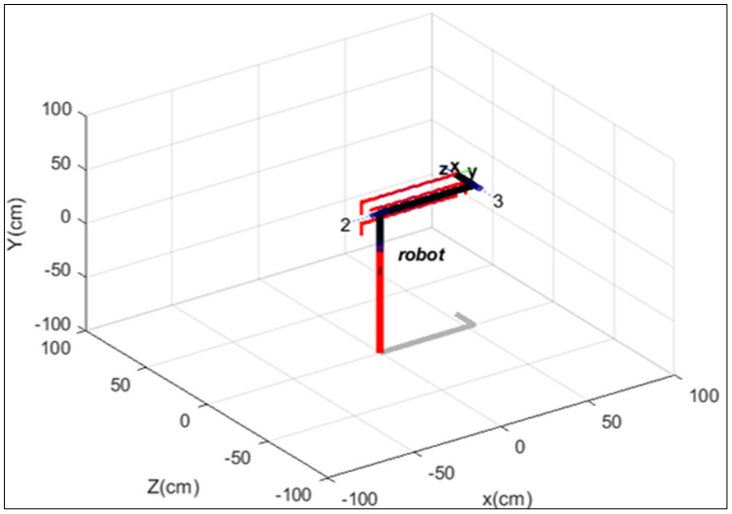

Fig. 19. Path of two cycles.

4.3.2 Dynamic model response

To simulate the behavior of each joint space of the robot, input the parameters from table 9 of the state-space were modelled (eq. 13) in MATLAB Simulink.

Table 9,
Parameters of dynamic model.

Parameter	Value
$(m_1 + m_2 + m_3)$	2.4 kg
$(m_2 + m_3)$	1 kg
m_3	0.8 kg
Stiffness coefficient(K_2)	0.53N/m
Damper coefficient of screws[13]	0.0064 N.s/m
Damper coefficient of belt	0.000001N.s/m
F_1	4.365N
F_2	0.1429N
F_3	1.26N
$(m_1 + m_2 + m_3)g$	23.544N

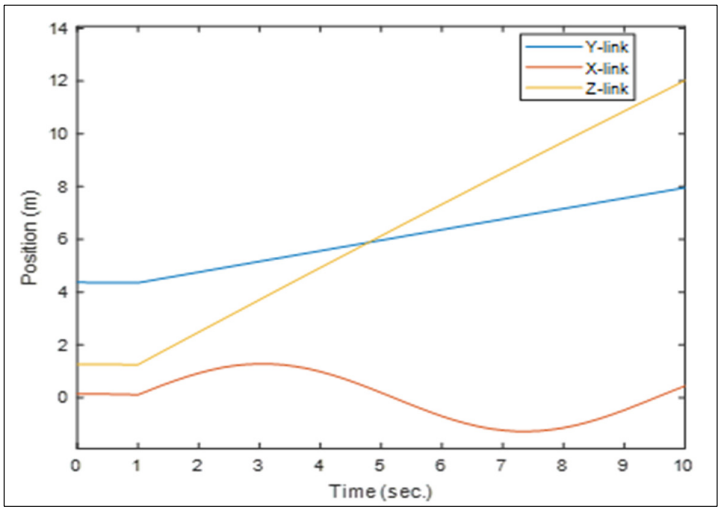

Fig. 20. First response of end-effector position.

Figure20 represents the system's response; the blue line is the end-effector's position in the Y-direction, the red line is the end-effector's position in the X-direction, and the yellow line is the end-effector's position in the Z-direction. As shown, X-position oscillates because of the spring effect (stiffness) created by the reaction of the belt. Figure21 represents the response of the system when value is neglected. Therefore, we notice the position in the Y-link increasing because the applied force is rising after the weight of the links is neglected.

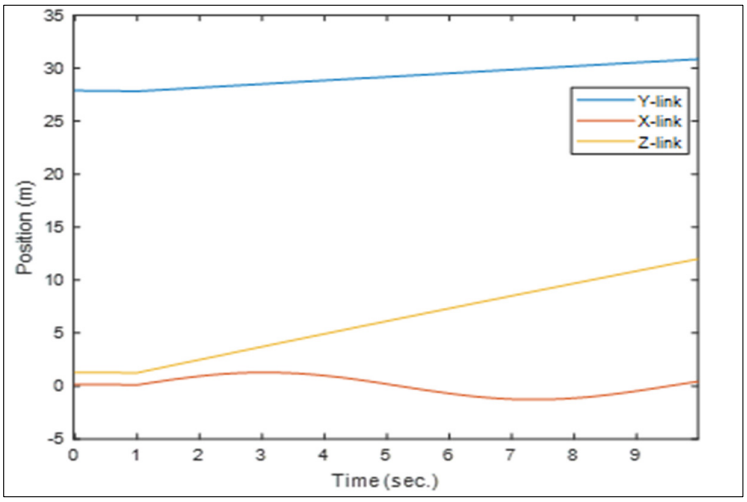

Fig. 21. Second response of end-effector position.

4.3.3 Experimental result

When running the robot, position and velocity with time have been calculated for link X-direction (second link) with a belt transformation element and Z-direction (Last link) with a screw transformation element. The motion starts from the initial position, as shown in fig. 22; the second link moves gradually in the X-direction for 1.2 seconds for the transient time of the robot system to get a steady state. After that, this link moves at a constant velocity, as shown in Fig 23.

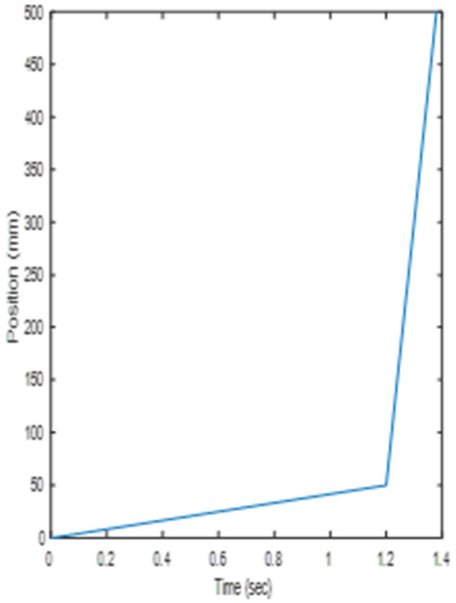

Fig. 22. X-position result for the second link.

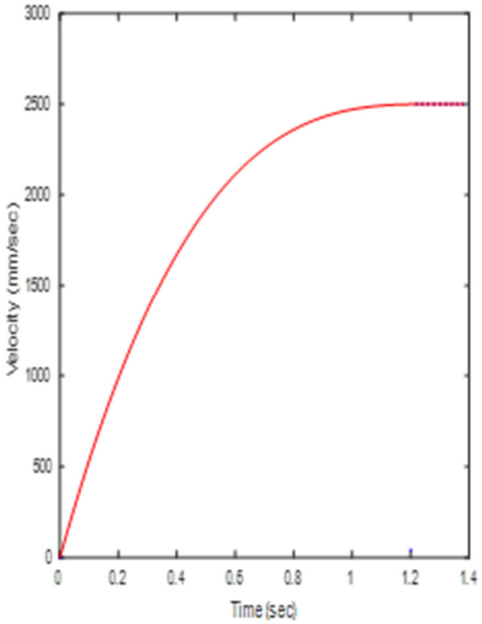

Fig. 23. Velocity for the second link.

While in the Z-direction, the motion starts from an initial position until 500 mm, as shown in fig. 24, the last link moves for 13.55 seconds. This time is low compared with the X-direction's motion because the previous link moves the screw slowly at 3.3 mm/sec. Fig. 25 shows that the velocity moves from zero until it reaches the maximum velocity, and it decreases to zero after getting to the final position.

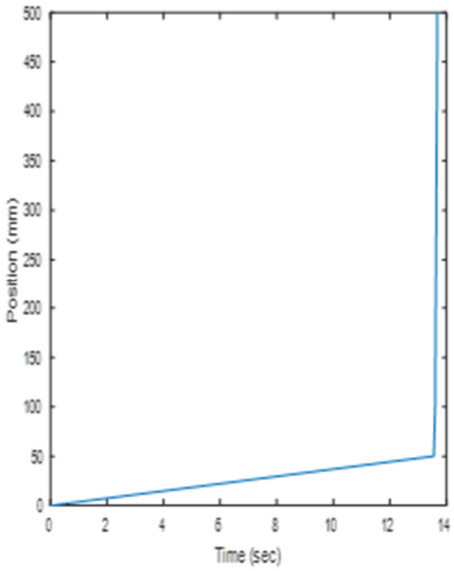

Fig. 24. Z-position result for the third link.

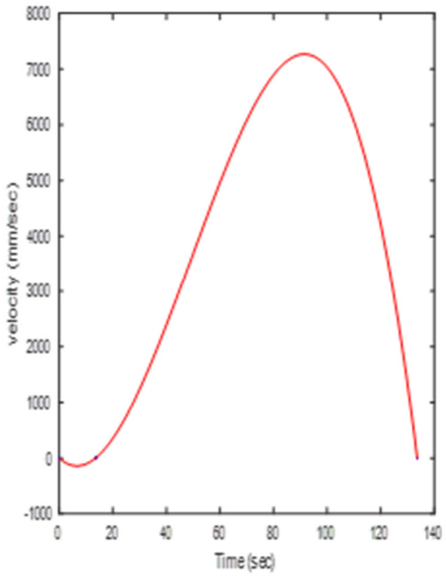

Fig. 25. Velocity for the third link.

Figure26 represents the difference between the response of a dynamic system model (measurement data) and the experimental results when running the robot; the blue line is the end-effector's position in the Z-direction when computing the system's parameters and the red line is the actual result of end-effector's position in the Z-direction.

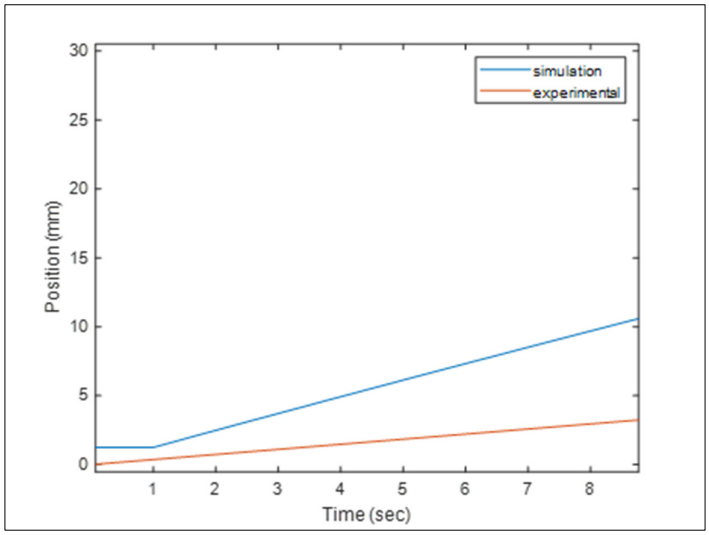

Fig. 26. Comparison between dynamic model and experimental result of Z-position.

Figure 27 also shows the same difference but for the end-effector's position in the X-direction. As shown the blue line is linear, the robot actually moves smoothly in the X-direction as shown.

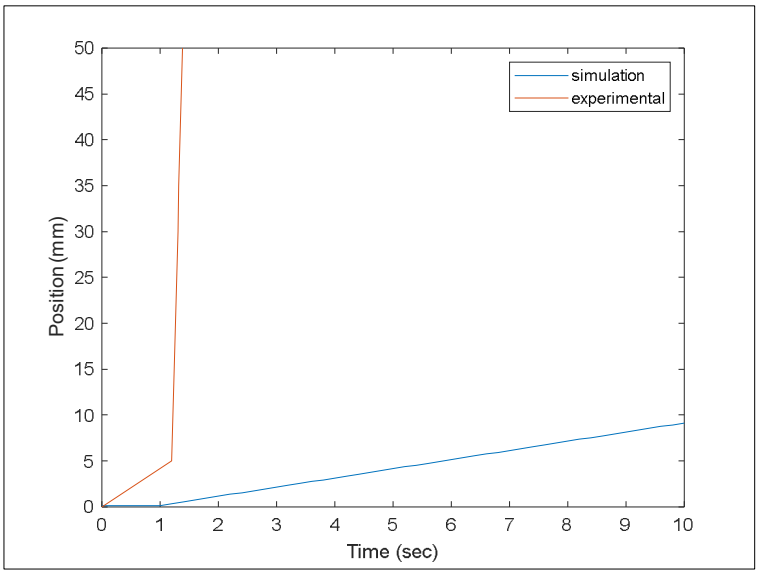

Fig. 27. Comparison between dynamic model and experimental result of X-position.

5. Conclusion

Compared to manual painting, the robotic spraying system has achieved optimal durability, safety, efficiency, and ease of use. All of the goals set for the proposed spraying robot have-been completed. The x-axis, y-axis, z-axis, and end-effector modules were all properly developed and built-in terms of mechanical design. All motors are mountings and couplings, and they are

correctly adjusted. All of the prismatic joints were successfully developed.

The structure is designed with sturdy and flexible arms to move smoothly, and the stress values for each link have been adjusted to ensure that the weights are handled to prevent bending and abrasion. The power systems module and the ARDUINO-NANO controller were successfully created in electrical and electronic systems. The software effectively controlled each joint of the spraying robot that completed the appropriate path for painting the wall. According to the experiment results, the proposed robot could move quickly in both vertical and horizontal motions.

In future work, a Raspberry pi controller could be used instead of an Arduino-Nano controller. Also, a machine vision and a camera are mounted on the robot to visualize and map for the path of the end-effector and to detect the windows and the door.

6. References

[1] Chen, Wei, and Dean Zhao. "Path Planning for Spray Painting Robot of Workpiece Surfaces." *Mathematical Problems in Engineering*, vol. 2013, 2013, pp. 1–6., https://doi.org/10.1155/2013/659457.

[2] Aris, Ishak Bin, and A. K. Iqbal. "Design and Fabrication of a Cartesian Painter Robot for the Construction Industry." International Journal of Mechanical Engineering Education, vol. 34, no. 2, 2006, pp. 125–144.

[3] Sorour, Mohamed. "RoboPainter–a conceptual towards robotized interior finishes." (2015).

[4] Scalera, Lorenzo, et al. "Airbrush Robotic Painting System: Experimental Validation of A Colour Spray Model." Advances in Service and Industrial Robotics, 2017, pp. 549–556., https://doi.org/10.1007/978-3-319-61276-8_57.

[5] Tuli, Tadele Belay. "Mathematical modeling and dynamic simulation of gantry robot using bond graph." International Conference on Information and Communication Technology for Develoment for Africa. Springer, Cham, 2017.

[6] Katsumata, Takuma, et al. "Optimal Exciting Motion for Fast Robot Identification. Application to Contact Painting Tasks with Estimated External Forces." Robotics and Autonomous Systems, vol. 113, 2019, pp. 149–159.

[7] N. Patel and R. Sarvaiya, "STUDY OF MATERIAL CHARACTERISTICS FOR EFFICIENT DESIGN OF SPRAY PAINTING ROBOT,", International Research Journal of Engineering and Technology (IRJET), Vol.07, Issue03, 2020.

[8] Muneer, Amgad, and Zhan Dairabayev. "Design and Implementation of Automatic Painting Mobile Robot." IAES International Journal of Robotics and Automation (IJRA), vol. 10, no. 1, 2021, p. 68.

[9] SPONG, Mark W., et al. Robot modeling and control. New York: Wiley, 2020.

[10] Siciliano, Bruno, et al. Force control. Springer London, 2009.

[11] Ljung, Lennart, and Torkel Glad. Modeling of dynamic systems. Prentice-Hall, Inc., 2002.

[12] Khurmi, R. S., and J. K. Gupta. A Textbook of Machine Design. Eurasia Publishing House, 2005.

[13] Ansoategui, Igor, and Francisco J. Campa. "Mechatronics of a Ball Screw Drive Using an N Degrees of Freedom Dynamic Model." The International Journal of Advanced Manufacturing Technology, vol. 93, no. 1-4, 2017, pp. 1307–1318.

[14] Tahseen F. Abaas, Ali A. Khleif, and Mohanad Q. Abbood, " Inverse Kinematics Analysis and Simulation of a 5 DOF Robotic Arm using MATLAB," Al-Khwarizmi Engineering Journal, Vol. 16, P. P. 1- 10 , March, (2020).

[15] Iman S. Karem, Talal A. Jabbar A.Wahab, and Mawadah J. Yahyh. "Design and Implementation for 3-DoF SCARA Robot based PLC," Al-Khwarizmi Engineering Journal, Vol. 13, No. 1, P.P. 40- 50 (2017).

[16] Maryam Sadeq Ahmed, and et al. "Robust Computed Torque Control for Uncertain Robotic Manipulatorss." Al-Khwarizmi Engineering Journal, vol. 17, no. 3, 2021, pp. 22–28., https://doi.org/10.22153/kej.2021.09.002.

تصميم وتحليل روبوت الرش

فاطمة محمد جاسم* مالك محمد علي**
علي حسين حمد***
*،**قسم هندسة الميكاترونيكس/ كلية الهندسة الخوارزمي/ جامعة بغداد*
*** قسم هندسة الاتصالات والمعلومات/ كلية الهندسة الخوارزمي/ جامعة بغداد*
*البريد الالكتروني: fatomaa.eng@gmail.com
**البريد الالكتروني: malik@kecbu.uobaghdad.edu.iq
***البريد الالكتروني: ahamad@kecbu.uobaghdad.edu.iq

الخلاصة

تم بناء روبوت رش داخلي في هذا البحث لحل العديد من المشاكل المرتبطة بالرش اليدوي. تم تفصيل وتصميم التقنيات الميكانيكية والأجهزة والتقنيات الأساسية المستخدمة. ينقسم التصميم التصوري لروبوت الرش المقترح إلى جزأين: الأجهزة والبرامج. يتم وصف التصميم الميكانيكي والتصنيع والأنظمة الكهربائية والإلكترونية في جزء الأجهزة، بينما يتم وصف التحكم في الروبوت في قسم البرنامج. تم تطوير النماذج الحركية والديناميكية لهذا الروبوت باستخدام ثلاثة روابط تتحرك في اتجاهات (x , y , z) .تم تصميم الروبوت بعد ذلك باستخدام برنامج SolidWorks لحساب انحراف كل اتصال والضغوط القصوى. أخيرًا، تم استخدام وحدة تحكم Arduino-Nano والمحركات المتدرجة لبناء وتشغيل الروبوت. ونتيجة لذلك، تمكن الروبوت من التحرك بسلاسة عموديًا وأفقيًا، وفقًا لنتائج التجارب.